Available online at www.sciencedirect.com
SCIENCE DIRECT®
Journal of Solid State Chemistry 178 (2005) 2586–2593
JOURNAL OF SOLID STATE CHEMISTRY
www.elsevier.com/locate/jssc

A structural study of the perovskite series $Na_{0.75}Ln_{0.25}Ti_{0.5}Nb_{0.5}O_3$

Roger H. Mitchell*, Ruslan P. Liferovich[1]

Department of Geology, Lakehead University, 955 Oliver Road, Thunder Bay, Ont., Canada P7B 5E1

Received 6 December 2004; received in revised form 26 April 2005; accepted 15 May 2005
Available online 14 July 2005

Abstract

The ternary stoichiometric perovskite compounds, $Na_{0.75}Ln_{0.25}Ti_{0.5}Nb_{0.5}O_3$ (*Ln* = La, Pr, Nd, Sm, Eu, Gd, Tb, Dy, Ho, Er, Tm) are intermediate members of the $NaNbO_3$–$Na_{0.5}Ln_{0.5}TiO_3$ solid solution series. The compounds were synthesized by standard ceramic methods at 1300 °C followed by annealing at 800 °C and quenching to ambient conditions. Rietveld analysis of the powder X-ray diffraction patterns shows that the compounds with *Ln* ranging from Pr to Tm adopt the orthorhombic space group *Pbnm* ($a \approx b \approx \sqrt{2}a_p$; $c \approx 2a_p$; $Z = 4$) and the $GdFeO_3$ structure. In contrast, $Na_{0.75}La_{0.25}Ti_{0.5}Nb_{0.5}O_3$ adopts the orthorhombic space group *Cmcm* ($a \approx b \approx c \approx 2a_p$; $Z = 4$). All cations located at the *A*- and *B*-sites are disordered in these compounds. The unit cell parameters and cell volumes of the compounds decrease regularly with increasing atomic number of the *Ln* cation. The *Pbnm* compounds with *Ln* from Sm to Tm have *A*-site cations in eight-fold coordination. *A*-site cations in the Pr and Nd compounds are considered to be in ten-fold coordination. Analysis of the crystal chemistry of the *Pbnm* compounds shows that *B*-site cations enter the second coordination sphere of the *A*-site cations for compounds with *Ln* from Tb to Tm as the *A*–*B* intercation distances are less than the maximum *A*–^{II}O(2) bond lengths. The [111] tilt angles of the $(Ti,Nb)O_6$ polyhedra in the *Pbnm* compounds increase with increasing atomic number from 11.1° to 15.8° and are less than those observed in lanthanide orthoferrite and orthoscandate perovskites. These data are considered as relevant to the sequestration of lanthanide fission products in perovskite and the structure of lanthanide-bearing perovskite-structured minerals.

Keywords: Perovskite; Lanthanides; Sodium niobate; Powder X-ray diffraction; Rietveld refinement; Coordination analysis

1. Introduction

The ability of the ABO_3 perovskite structure to host a variety of elements at both of the cation sites is due the high tolerance of the structure to distortions [1]. Typically, substitution of cations of differing size at the *A*- and *B*-sites reduces the symmetry from that of the $Pm\bar{3}m$ aristotype to tetragonal, orthorhombic and monoclinic derivatives. Substitution of cations of similar size in distorted derivatives commonly does not cause a change in space group but can result in changes in cell dimensions, tilt angles of BO_6 polyhedra and displacement of *A*-cations. These changes can produce significant variations in physical properties. Thus, the complex lanthanide-bearing perovskites, $(Na,Ln)Ti_2O_6$, have been investigated to determine the changes in their structures with respect to *Ln*-substitutions at the *A*-site [2,3].

Perovskite-structured oxides are significant constituents of SYNROC [4], a multiphase ceramic composite that has been proposed for the sequestration of radioactive waste. Lanthanide-bearing perovskites are of interest in this respect because lanthanides occur as fission products, and because Gd^{3+} has been regarded as a crystallochemical analog of Pu^{3+} [5]. Thus, data on the structure of lanthanide-bearing perovskites are of

*Corresponding author. Fax: +1 807 346 7853.
E-mail address: rmitchel@lakeheadu.ca (R.H. Mitchell).
[1]Permanent address: Geological Institute Kola Science Centre, Russian Academy of Sciences, 14 Fersman Street, Apatity 184200, Russia.

0022-4596/$ - see front matter © 2005 Elsevier Inc. All rights reserved.
doi:10.1016/j.jssc.2005.05.016

interest with respect to the perovskite solid solutions expected to be formed in the SYNROC process.

Studies of the crystal structures of solid solutions involving $NaNbO_3$ and $NaLnTi_2O_6$ are important with respect to the above problems and to the crystal chemistry of naturally-occurring perovskite group compounds. These minerals are commonly complex solid solutions between $NaNbO_3$, $NaLnTi_2O_6$, $CaTiO_3$ and $SrTiO_3$. To date few of their structures have been determined because of the twinned character and compositional heterogeneity of most crystals. Thus, recourse must be made to the study of synthetic analogs as an aid to understanding their crystal chemistry [1].

Sodium niobate ($NaNbO_3$) exhibits a series of phase transitions as a function of temperature change. The space groups of these polymorphs are not well-defined but range from $R3c$ ($<-80\,^{\circ}C$) through an undetermined monoclinic space group (-80 to $370\,^{\circ}C$), undetermined orthorhombic (370–480 °C), undetermined orthorhombic (480–520 °C), orthorhombic $Cmcm$ (520–575 °C), tetragonal $P4/mbm$ (575–640 °C) to cubic $Pm\bar{3}m$ ($>640\,^{\circ}C$) [6]. Note that although the space group of the structure adopted at -80 to $370\,^{\circ}C$ is normally considered to be orthorhombic $Pbma$ [7], the high resolution neutron diffraction data of [6] clearly show this to be incorrect.

The $NaLnTi_2O_6$ (Ln = Pr–Lu) compounds adopt the orthorhombic space group $Pbnm$ (#62; cab setting) [2,3]. In contrast, $NaLaTi_2O_6$ has rhombohedral symmetry and adopts space group $R\bar{3}c$ [2,8] because of the large size of the La^{3+} cation relative to the other lanthanides. There are no data on the phase transitions of the $NaLnTi_2O_6$ compounds.

It is well known that solid solutions of $NaNbO_3$ with other perovskite-structured compounds result in changes in space group as a function of composition [1,9], and that subtle changes in the coordination environment of lanthanide cations in the $LnFeO_3$ [10] and $LnScO_3$ [11] solid solution series occur as consequence of small changes in lanthanide ionic radius. Hence, we can expect similar structural complexity in the solid solution series $(NaNbO_3)_{1-x}(NaLnTi_2O_6)_x$ ($0<x<1$). As a preliminary to the investigation of this system we have investigated the crystal structures of the $x = 0.5$ compounds to document the changes in the structure and coordination environment of the A- and B-site cations as a function of lanthanide cation radius and replacement of Nb by Ti.

2. Experimental methods

Compositions corresponding to $Na_{0.75}Ln_{0.25}Ti_{0.5}Nb_{0.5}$, where Ln = La to Lu, were synthesized at ambient pressure from stoichiometric amounts of Na_2CO_3, TiO_2, Nb_2O_5 and the relevant Ln_2O_3 oxides, Tb_7O_{12}, Pr_6O_{11}, Y_2O_3 and CeO_2 (all high purity grade Alfa Aesar Co., reagents). Na_2CO_3 was taken in 10 mol% excess to compensate for volatilization of sodium, and 5 wt% graphite was added to the Tb, Pr and Ce-bearing samples for reduction at the calcination stage.

All reagents were dried in at 120 °C and mixed in an agate mortar under acetone, followed by calcination in air for 24 h at 1000 °C. After regrinding, the samples were pelletized at a pressure of 10 ton/cm^2, and sintered in air for 24 h at 1100 °C. Subsequently, the samples were reground, repelletized, sintered for 48 h at 1300 °C, quenched to 800 °C and annealed at this temperature for 48 h, before quenching to room temperature.

Step scanned powder X-ray diffraction (XRD) patterns of the experimental products were obtained at room temperature using a Philips 3710 diffractometer (Cu$K\alpha$ radiation; 2θ range 10–145°; $\Delta 2\theta$ 0.02°; time per step 4 s; graphite monochromator).

The XRD patterns were inspected using the Bruker AXS software package EVA to identify the phases present, and confirm that perovskite-structured compounds were formed. Data were analysed by Rietveld methods using the Bruker AXS software package TOPAS 2.1 operated in the fundamental parameters mode [12]. Data were corrected for Lorenz and polarization effects. Refined parameters included: zero corrections, scaling factors, cell dimensions, atomic positional coordinates, preferred orientation corrections, strain effects and isotropic thermal parameters (B_{iso}).

The IVTON program [13] was employed to characterize the coordination spheres of the A and B-site cations, obtain bond lengths, volumes of coordination polyhedra, and displacements of cations from the centers of coordination polyhedra. The geometry of cation coordination polyhedra is described in terms of the polyhedron bond length distortion index (Δ_n) and the bond angle variance index (δ_n) as formulated by Shannon [14] and Robinson et al. [15], respectively. The ATOMS 6.0 software package [16] was used to determine interaxial angles describing the distortion of BO_6 octahedra. Tilt angles of BO_6 polyhedra for $Pbnm$-structured compounds were calculated from the bond angles B–O(1)–B and B–O(2)–B following [17], and from anion coordinates following [18] for the $Cmcm$ structured La-compound.

3. Experimental results

Synthesis of $Na_{0.75}Ln_{0.25}Ti_{0.5}Nb_{0.5}O_3$ compounds was attempted for all of the lanthanides and yttrium. The experiments resulted in the formation of a perovskite-structured oxide as a single phase for La, Pr, Nd, Sm, Eu, Gd, Tb, and Dy. For Ho, Er and Tm, the products contained ~1 wt% of a Ln-pyrochlore. Compositional

data and Rietveld refinement confirmed that the dominant perovskite phase was stoichiometric. Pyrochlore-structured phases become more abundant in the synthesis of the Lu, Yb and Y compounds, and comprise 4–9 wt% of the run products. Compositional data showed that these perovskites deviated significantly in their composition from the expected stoichiometry. Thus, these compounds are not considered further here. The experiments involving Ce did not produce any perovskite-structured compounds due to the oxidation of Ce.

3.1. Rietveld refinement

Inspection of the powder XRD patterns indicated that the La compound adopts a different space group to all of the other compounds synthesized. This is clearly evident from Fig. 1 which compares the diffraction patterns of the La, Pr and Nd compounds in the 85–92° 2θ range, and shows that the reflection at 86–87° 2θ is a single peak for the La compound and doublet for the Pr and Nd compounds. The diffraction patterns of the Sm, Eu, Gd, Tb, Dy, Ho, Er and Tm compounds exhibit the same doublet.

Possible space groups for the La compound include *Cmcm*, *Imma* and *Pbnm*. Although perovskites adopting *Cmcm* and *Pbnm* space groups are common and easily recognized by laboratory XRD methods, those adopting the *Imma* space group are considered to be "rare". However, this apparent "rarity" might reflect the inherent limitations of laboratory powder XRD methods, as high resolution neutron diffraction has demonstrated that compounds formerly considered to adopt *Cmcm* symmetry e.g., $SrZrO_3$ at 1023–1113 K [19] actually have *Imma* structures. Similarly, synchrotron XRD has shown that high temperature phases of $SrRhO_3$ [20], $SrRuO_3$ [21], and some compounds in the $Sr_{1-x}Ba_xHfO_3$ series [22] also adopt *Imma* symmetry. Typically, laboratory powder XRD, as used in this work, does not record the very low intensity superlattice peaks which aid in the recognition of *Imma* symmetry, although *M* and *R*-point reflections are recognizable for the *Pbnm* structured compounds. Thus, the identification of the space group of the La-compound synthesized here is based primarily on splitting of the lattice peaks. Attempts to fit the powder XRD pattern of the La compound to an *Imma* structure resulted in a very poor fit (GoF = 2.78; R_{wp} = 19.68; DW = 0.46; R_{Bragg} = 12.1%) and significant residuals at high diffraction angles (Fig. 2a). A better, but still unacceptable, poor fit was obtained for the *Pbnm* space group (GoF = 1.90; R_{wp} = 13.43; DW = 0.67; R_{Bragg} = 7.3%). A satisfactory fit was obtained only for *Cmcm* (Table 1; Fig. 2b).

Following [23,24], the single peak at 86.47° 2θ for the La compound is ascribed to the 4 4 4 reflection in the orthorhombic space group *Cmcm*, and the doublet at 86.75° and 87.01° 2θ to the 0 4 4 and 4 0 4 reflections in the orthorhombic space group *Pbnm*, respectively. Thus, we consider $Na_{0.75}La_{0.25}Ti_{0.5}Nb_{0.5}$ to adopt the space group *Cmcm* (#63) and all other compounds synthesized to have *Pbnm* (#62: *cab* setting) structures.

We used the atomic coordinates given by Kennedy et al. [23] as a starting model for the refinement of the

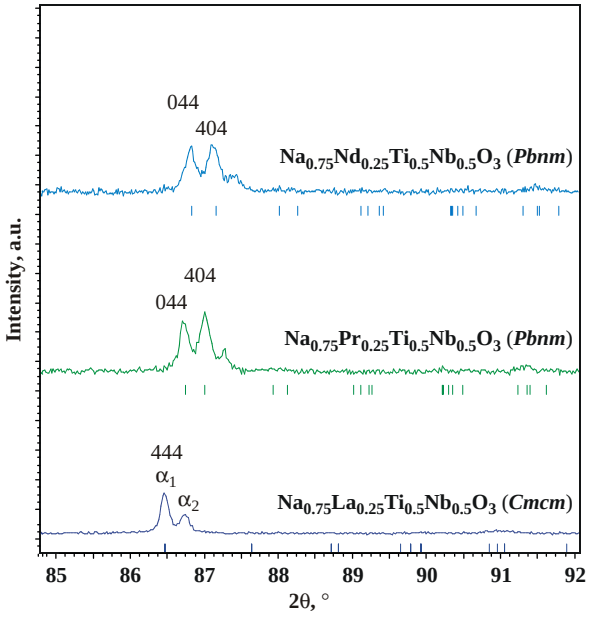

Fig. 1. Powder X-ray diffraction patterns for the La, Pr and Nd compounds in the 2θ region 85–92°.

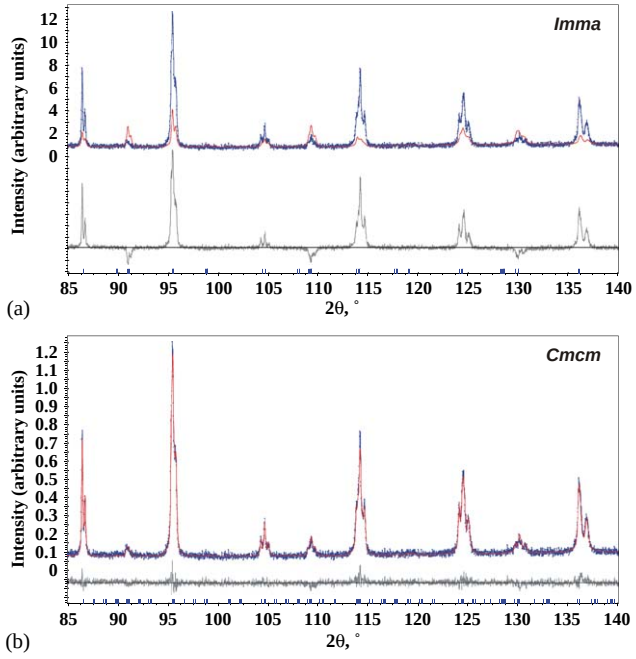

Fig. 2. Observed and difference profiles for Rietveld refinements of powder X-ray diffraction patterns for $Na_{0.75}La_{0.25}Ti_{0.5}Nb_{0.5}O_3$ (a) in the space group *Imma* (b) in the space group *Cmcm*. The bars indicate the allowed Bragg reflections for each space group.

Table 1
Crystallographic characteristics of $Na_{0.75}La_{0.25}Ti_{0.5}Nb_{0.5}O_3$ perovskite adopting the space group *Cmcm*

	x	*y*	*z*	B_{iso}
(Na,La)1	0	0.005(2)	1/4	1.5(2)
(Na,La)2	0	0.494(2)	1/4	1.1(2)
(Nb,Ti)	1/4	1/4	0	0.45(2)
O(1)	0.251(3)	0	0	2.1(1)
O(2)	0	0.225(2)	0.012(4)	2.1(1)
O(3)	0.284(2)	0.261(5)	1/4	2.1(1)

Unit-cell parameters: $a = 7.7827(2)$, $b = 7.7864(2)$, $c = 7.8039(1)$ Å, $V = 472.91(2)$ Å^3; final agreement factors: $R_{wp} = 9.51$, $R_{exp} = 7.07$, $R_{Bragg} = 3.42$, DW = 1.20, GoF = 1.34; $^{xii}R_A^{3+} = 1.382$ Å, $^{vi}R_B = 0.623$ Å, $^{xii}t = 0.970$.

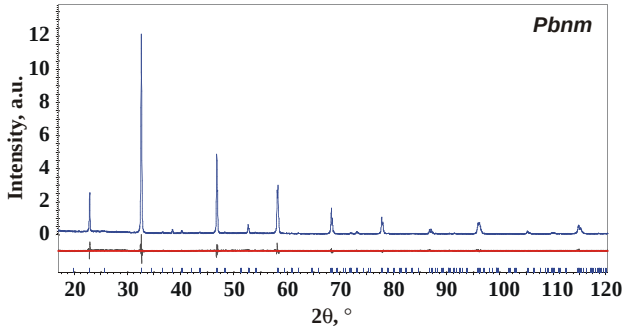

Fig. 3. Rietveld refinement plot of the powder diffraction data for $Na_{0.75}Gd_{0.25}Ti_{0.5}Nb_{0.5}O_3$. The bars indicate the allowed Bragg reflections for *Pbnm* structure. For details of the refinement, see text and Table 3.

structure of *Cmcm* La-compound. The atomic coordinates of the lanthanide orthoferrites given by Marezio et al. [10] were used as starting models for the refinement of the structures of the *Pbnm* compounds $Na_{0.75}Ln_{0.25}Ti_{0.5}Nb_{0.5}O_3$ (*Ln* = *Pr*, Nd, Sm, Eu, Gd, Tb, Dy, Ho, Er, Tm). Fig. 3 illustrates a portion of the powder XRD pattern and Rietveld difference plot for $Na_{0.75}Gd_{0.25}Ti_{0.5}Nb_{0.5}O_3$.

4. *Cmcm* $Na_{0.75}La_{0.25}Ti_{0.5}Nb_{0.5}O_3$

Cell dimensions and atomic coordinates for *Cmcm* $Na_{0.75}La_{0.25}Ti_{0.5}Nb_{0.5}$ are given in Table 1. The structure of this compound consists of tilted $(Ti,Nb)O_6$ polyhedra with the Na^+ and La^{3+} cations randomly distributed in two 12-fold coordinated interstitial sites, $A(1)O_{12}$ and $A(2)O_{12}$ (Table 2). *Cmcm*-structured perovskites can be considered as being derived from a $Pm\bar{3}m$ aristotype by unequal out-of-phase (b^-) and in-phase (c^+) tilting of the $(Ti,Nb)O_6$ polyhedra about the cubic [0 1 0] and [0 0 1] axes. This tilt scheme in the notation of [25] is $a^0b^-c^+$. Rotation angles calculated

Table 2
Crystal chemistry and selected interatomic distances and angles of $Na_{0.75}La_{0.25}Ti_{0.5}Nb_{0.5}O_3$ perovskite adopting the space group *Cmcm*

AO_{12} polyhedra			BO_6 polyhedron		
$A(1)O_{12}$	(Å^3)	47.30(4)	BO_6	(Å^3)	9.920(3)
$\langle A(1)-^{[1]}O\rangle$	(Å)	2.712(23)	$\langle B-O\rangle$	(Å)	1.958(2)
$\Delta(1)_{12}$		3.191	Δ_6		0.025
$2\times A(1)$–O2	(Å)	2.524(25)	$2\times B$–O1	(Å)	1.947(0)
$2\times A(1)$–O3	(Å)	2.536(36)	$2\times B$–O2	(Å)	1.958(2)
$2\times A(1)$–O2′	(Å)	2.720(25)	$2\times B$–O3	(Å)	1.971(3)
$4\times A(1)$–O1	(Å)	2.758(14)	Δ_6		0.025
$2\times A(1)$–O3′	(Å)	2.977(29)			
$d_{A(1)}$		0.012	$2\times$ O1–*B*–O2	(deg)	92.5(2)
$\Delta x_{A(1)}$		0	$2\times$ O1–*B*–O2	(deg)	84.4(2)
$\Delta y_{A(1)}$		0.0015	$2\times$ O1–*B*–O2	(deg)	84.7(2)
			$2\times$ O1–*B*–O2	(deg)	95.6(2)
$A(2)O_{12}$	(Å^3)	52.18(4)	$2\times$ O2–*B*–O2	(deg)	95.3(2)
$\langle A(2)-^{[1]}O\rangle$	(Å)	2.806(22)	$2\times$ O2–*B*–O2	(deg)	87.5(2)
$\Delta(2)_{12}$		3.191	*B*–O1–*B*	(deg)	179.77
$d_{A(2)}$		0.076	*B*–O2–*B*	(deg)	167.26
$\Delta x_{A(2)}$		0	δ_6		23.77
$\Delta y_{A(2)}$		−0.0098	b^-	(deg)	5.26
			c^+	(deg)	2.98
$2\times A(2)$–O3	(Å)	2.673(32)			
$4\times A(2)$–O1	(Å)	2.753(14)			
$2\times A(2)$–O2	(Å)	2.798(24)			
$2\times A(2)$–O3′	(Å)	2.861(27)			
$2\times A(2)$–O2′	(Å)	2.996(24)			

from atomic coordinates of the oxygen anions [23] are 5.26° and 2.98° for the out-of-phase and in-phase tilts, respectively. These relatively small tilt angles, together with the retention of 12-fold coordination for the *A*-site cations, indicates the structure is only slightly distorted from that of the cubic aristotype. In this respect, the Goldschmidt tolerance factor for 12-fold *A*-site coordination ($^{xii}t = 0.97$) for this compound is close to unity. Evidently the large size of the La^{3+} cation relative to those of the other lanthanides inhibits reduction of the symmetry to the three-tilt *Pbnm* space group observed for other compounds synthesized (see below).

Crystallochemical data for *Cmcm* $Na_{0.75}La_{0.25}Ti_{0.5}Nb_{0.5}$ are given in Table 2. The $(Ti,Nb)O_6$ polyhedron ($V = 9.920(3)$ Å^3) is only slightly distorted ($\Delta_B = 0.025$), although the bond angle distortion is high ($\delta_B = 23.77$) due to the O_i–*B*–O_j bond angles ranging from 84.4(4)° to 95.6(2)°. Similar styles of distortions have been described for *Cmcm* $SrZrO_3$ ($\Delta_B = 0.006$, $\delta_B = 10.61$) and $SrHfO_3$ ($\Delta_B = 0.007$, $\delta_B = 8.63$) [18,24]. The $A(1)O_{12}$ and $A(2)O_{12}$ polyhedra have volumes of 47.30(4) Å^3 and 52.18(4) Å^3, with mean $\langle A-O\rangle$ bond lengths of 2.71(2) Å and 2.81(2) Å, respectively. The bond length distortion index is 3.19 for both polyhedra. The [0,*b*,0] displacement ($d_{A(1)}$) of the *A*(2) cation is 0.08 Å, whereas the *A*(1) cation is close to the geometrical center of the coordination polyhedron ($d_{A(2)} = 0.01$ Å).

Table 3
Crystallographic characteristics of $Na_{0.75}Ln_{0.25}Ti_{0.5}Nb_{0.5}O_3$ perovskites adopting the space group *Pbnm*

Ln		Pr	Nd	Sm	Eu	Gd	Tb	Dy	Ho	Er	Tm
$^{viii}R_A^{3+}$		1.167	1.162	1.155	1.152	1.148	1.145	1.142	1.139	1.136	1.134
$^{vi}R_B$		0.623	0.623	0.623	0.623	0.623	0.623	0.623	0.623	0.623	0.623
^{viii}t		0.895	0.894	0.891	0.890	0.889	0.888	0.887	0.886	0.885	0.884
$^{viii}t_o$		0.940	0.936	0.929	0.927	0.921	0.913	0.911	0.910	0.901	0.902
a(Å)		5.4771(1)	5.4690(1)	5.4506(1)	5.4424(1)	5.4338(1)	5.4237(1)	5.4157(2)	5.4082(2)	5.3977(1)	5.3930(1)
b(Å)		5.4968(1)	5.4934(1)	5.4884(1)	5.4871(1)	5.4880(1)	5.4860(1)	5.4835(2)	5.4884(2)	5.4860(1)	5.4861(1)
c(Å)		7.7655(1)	7.7569(1)	7.7417(2)	7.7345(2)	7.7284(2)	7.7191(2)	7.7115(2)	7.7096(3)	7.7008(2)	7.6975(1)
V(Å^3)		233.79(1)	233.04(1)	231.59(1)	230.97(1)	230.46(1)	229.68(9)	229.01(1)	228.84(1)	228.03(1)	227.74(1)
A:	x_A	0.9950(11)	0.9956(10)	0.9944(10)	0.9934(9)	0.9933(9)	0.9931(8)	0.9919(10)	0.9913(10)	0.9917(6)	0.9910(6)
	y_A	0.0162(5)	0.0187(4)	0.0235(5)	0.0262(5)	0.0295(4)	0.0328(4)	0.0340(4)	0.0353(5)	0.0418(3)	0.0428(3)
	z_A	1/4	1/4	1/4	1/4	1/4	1/4	1/4	1/4	1/4	1/4
	B(Å^2)	0.90(3)	0.90(3)	1.27(4)	1.24(4)	1.21(4)	0.95(4)	1.27(4)	1.61(7)	1.21(4)	1.43(4)
	d_A	0.631	0.613	0.591	0.580	0.559	0.546	0.533	0.532	0.491	0.494
	Δx_A	0.0002	0.0012	0.0013	−0.0007	0.0006	0.0013	−0.0008	−0.0003	0.0011	−0.0005
	Δy_A	−0.1148	−0.1115	−0.1076	−0.1057	−0.1019	−0.0995	−0.0972	−0.0970	−0.0895	0.0900
B:	x_B	0	0	0	0	0	0	0	0	0	0
	y_B	1/2	1/2	1/2	1/2	1/2	1/2	1/2	1/2	1/2	1/2
	z_B	0	0	0	0	0	0	0	0	0	0
	B(Å^2)	0.58(2)	0.51(2)	0.61(2)	0.65(2)	0.49(2)	0.38(2)	0.41(2)	0.51(3)	0.44(2)	0.56(3)
O1:	x	0.0534(26)	0.0517(22)	0.0584(23)	0.0629(21)	0.0666(19)	0.0699(18)	0.0755(21)	0.0737(20)	0.0761(14)	0.0805(14)
	y	0.4889(22)	0.4865(18)	0.4890(20)	0.4897(18)	0.4864(17)	0.4861(16)	0.4838(18)	0.4857(20)	0.4831()	0.4853(13)
	z	1/4	1/4	1/4	1/4	1/4	1/4	1/4	1/4	1/4	1/4
	B(Å^2)	1.58(11)	1.34(9)	1.73(12)	1.67(11)	1.34(11)	1.18(11)	1.95(13)	1.63(2)	1.00(12)	1.00(12)
O2:	x	0.7291(23)	0.7275(19)	0.7222(19)	0.7264(18)	0.7206(15)	0.7173(14)	0.7210(17)	0.7161(15)	0.7126(11)	0.7158(12)
	y	0.2852(18)	0.2845(15)	0.2855(17)	0.2881(14)	0.2892(13)	0.2931(12)	0.2911(15)	0.2934(14)	0.2920(11)	0.2956(11)
	z	0.0290(13)	0.0326(10)	0.0339(11)	0.0339(11)	0.0350(10)	0.0387(9)	0.0398(10)	0.0390(10)	0.0452(7)	0.0413(7)
	B(Å^2)	1.58(11)	1.34(9)	1.73(12)	1.67(11)	1.34(11)	1.18(11)	1.95(13)	1.63(23)	1.00(12)	1.00(12)
R_{wp}		10.62	10.84	10.90	10.93	10.27	10.23	11.34	12.14	9.74	8.47
R_{exp}		7.76	7.82	7.49	7.54	7.51	7.46	7.54	6.49	5.91	5.42
R_{Bragg}		2.92	2.43	2.60	3.04	3.12	2.72	3.65	4.17	4.07	3.32
DW		1.14	1.07	1.01	0.98	1.12	1.16	0.92	0.65	0.82	0.91
GoF		1.37	1.39	1.45	1.45	1.37	1.37	1.50	1.87	1.65	1.56

Note. Standard deviations are given in parentheses. ^{viii}t Goldschmidt tolerance factor; $^{viii}t_o$ observed tolerance factor. Δx_A and Δy_A parameters in fractions of the unit cell dimensions describing displacement of A-site cation from the center of coordination polyhedron, d_A (Å).

Table 4
Crystal chemistry of $Na_{0.75}Ln_{0.25}Ti_{0.5}Nb_{0.5}O_3$ perovskites adopting the space group *Pbnm*

Ln	AO_8	Δ_8	A–^{I}O	A–^{II}O	BO_6	Δ_6	B–O	f-8	ΔV	AO_{12}	f-12	[1 1 0]	[0 0 1]	[1 1 1]	a_x^-
Pr	26.847(19)	2.022	2.612(12)	3.040(12)	10.102(10)	0.532	1.965(8)	2.66	21.50	48.35	4.79	8.75	6.79	11.06	6.19
Nd	26.724(15)	2.177	2.601(10)	3.056(11)	10.099(9)	0.383	1.965(7)	2.65	21.44	48.16	4.77	8.57	7.76	11.54	6.09
Sm	26.462(17)	2.300	2.583(11)	3.082(12)	10.114(9)	0.167	1.965(7)	2.62	21.32	47.78	4.72	10.50	5.93	12.04	7.44
Eu	26.248(16)	2.262	2.576(10)	3.091(11)	10.096(8)	0.561	1.964(7)	2.60	21.40	47.65	4.72	10.20	7.50	12.64	7.22
Gd	26.084(15)	2.401	2.562(9)	3.122(10)	10.147(7)	0.269	1.967(7)	2.57	21.39	47.47	4.68	10.85	8.03	13.47	7.68
Tb	25.803(14)	2.867	2.546(8)	3.153(10)	10.211(7)	0.311	1.972(5)	2.53	21.41	47.21	4.62	11.35	9.27	14.62	8.04
Dy	25.640(15)	3.029	2.540(10)	3.161(10)	10.194(8)	0.413	1.971(7)	2.52	21.42	47.06	4.62	12.25	8.32	14.77	8.68
Ho	25.645(15)	2.921	2.537(9)	3.167(10)	10.210(7)	0.275	1.971(7)	2.51	21.36	47.00	4.60	11.90	9.13	14.96	8.43
Er	25.438(11)	3.354	2.518(7)	3.164(7)	10.281(6)	0.086	1.976(5)	2.47	21.29	46.73	4.55	12.35	10.39	16.09	8.75
Tm	25.338(11)	2.965	2.518(6)	3.205(7)	10.243(6)	0.386	1.974(5)	2.47	21.36	46.69	4.56	12.90	9.21	15.81	9.14

Note. AO_8 and AO_{12} volumes (Å^3) of polyhedra with A-site cation in 8- and 12-fold coordination, respectively.
BO_6 is the volume (Å^3) of the BO_6 polyhedron. Δ_8 and Δ_6 are the distortion indices of the AO_8 and BO_6 polyhedra, respectively.
AO_{12} is the ideal volume of the A-site polyhedron which is calculated from V and BO_6. A–O^j and B–O are the mean bond lengths (Å) for the AO_8 and BO_6 polyhedra, respectively. A–^{I}O(1)-first and A–^{II}O(2) second coordination spheres of lanthanide ion. The volume of the second coordination sphere, ΔV, is AO_{12}–AO_8. Polyhedron volume ratios (V_A/V_B), f-12 and f-8, are for 8 and 12-fold coordinated A-site cations, respectively. [1 1 0], [0 0 1] and [1 1 1] are octahedral tilts angles (deg) and a_x^- is the [1 0 0] = [0 1 0] tilt angle (deg); all tilt angles are determined from bond angles.

5. *Pbnm*-structured $Na_{0.75}Ln_{0.25}Ti_{0.5}Nb_{0.5}O_3$ perovskites

Cell dimensions, atomic coordinates, bond lengths and other crystallographic characteristics of the $Na_{0.75}Ln_{0.25}Ti_{0.5}Nb_{0.5}$ compounds synthesized are given in Tables 3–5. With the exception of La, disordered ABO_3 $GdFeO_3$-type perovskites were formed from all lanthanides. The structure of these perovskites is derived

Table 5
Selected interatomic distances (Å) and angles (deg) in $Na_{0.75}Ln_{0.25}Ti_{0.5}Nb_{0.5}O_3$ perovskites adopting the space group *Pbnm*

Ln	Pr	Nd	Sm	Eu	Gd	Tb	Dy	Ho	Er	Tm
A–O1	2.478(15)	2.482(13)	2.445(14)	2.423(12)	2.403(11)	2.384(4)	2.359(12)	2.368(12)	2.355(8)	2.332(8)
A–O1	2.618(13)	2.588(10)	2.578(11)	2.571(10)	2.539(10)	2.521(9)	2.508(10)	2.512(10)	2.463(7)	2.475(7)
2 × *A*–O2	2.463(11)	2.447(9)	2.429(10)	2.436(9)	2.419(8)	2.386(7)	2.394(9)	2.380(8)	2.362(6)	2.380(6)
2 × *A*–O2	2.693(11)	2.669(9)	2.658(10)	2.640(9)	2.643(8)	2.634(8)	2.602(9)	2.621(9)	2.577(6)	2.590(6)
2 × *A*–O2	2.744(11)	2.754(9)	2.733(9)	2.733(9)	2.714(8)	2.712(7)	2.730(8)	2.707(8)	2.724(6)	2.699(6)
A–O1	2.916(12)	2.940(10)	2.954(11)	2.968(10)	3.007(10)	3.028(9)	3.051(10)	3.049(10)	3.082(8)	3.096(7)
A–O1	3.007(15)	2.998(13)	3.019(14)	3.034(13)	3.051(11)	3.064(11)	3.085(12)	3.068(12)	3.099(7)	3.098(8)
2 × *A*–O2	3.118(11)	3.142(9)	3.178(10)	3.181(9)	3.214(8)	3.260(7)	3.254(9)	3.275(8)	3.327(6)	3.313(6)
2 × *A*–B	3.293(2)	3.279(2)	3.254(2)	3.240(2)	3.225(2)	3.208(2)	3.201(2)	3.197(2)	3.166(1)	3.162(1)
2 × *B*–O1	1.964(2)	1.961(2)	1.962(2)	1.965(2)	1.967(2)	1.968(2)	1.973(2)	1.970(2)	1.971(2)	1.974(2)
2 × *B*–O2	1.910(12)	1.920(10)	1.936(10)	1.907(9)	1.928(8)	1.931(7)	1.921(9)	1.932(8)	1.957(6)	1.926(6)
2 × *B*–O2	2.021(11)	2.014(9)	1.998(10)	2.021(9)	2.007(8)	2.016(7)	2.019(9)	2.012(8)	2.001(6)	2.021(6)
O1–*B*–O1	180	180	180	180	180	180	180	180	180	180
2 × O1–*B*–O2	89.1(6)	89.6(4)	89.1(5)	89.9(4)	89.6(3)	89.0(4)	88.9(4)	89.8(3)	88.9(3)	89.0(3)
2 × O1–*B*–O2	90.9(6)	90.3(4)	90.4(4)	91.0(3)	90.8(4)	91.0(4)	91.1(4)	90.9(4)	91.1(3)	91.0(3)
2 × O1–*B*–O2	90.4(4)	92.4(4)	88.5(4)	89.0(3)	90.4(3)	89.9(3)	89.4(3)	89.1(3)	89.3(2)	90.4(2)
2 × O1–*B*–O2	89.6(4)	91.0(5)	90.9(5)	90.1(4)	90.9(3)	90.1(3)	90.6(3)	90.2(3)	90.7(2)	89.6(2)
2 × O2–*B*–O2	91.2(5)	89.7(4)	89.6(4)	90.7(4)	89.1(3)	91.2(3)	88.9(5)	90.9(3)	92.1(2)	90.6(3)
2 × O2–*B*–O2	88.9(5)	91.0(5)	91.5(4)	91.0(5)	89.2(4)	88.8(3)	90.1(4)	89.2(3)	87.9(2)	89.5(3)
B–O1–*B*	162.5	162.8	159.0	159.6	158.3	157.3	155.5	156.2	155.3	154.2
B–O2–*B*	161.6	160.3	161.0	159.2	157.8	155.5	156.0	155.2	152.9	154.1
δ_6	0.66	1.16	0.92	0.50	0.46	0.70	0.62	0.45	1.75	0.42

Note. δ_6 Octahedral bond angle variance on (*see text for explanation*).

from the cubic aristotype by three separate unequal rotations of the (Ti,Nb)O_6 polyhedra about the [1 0 0], [0 1 0] and [0 0 1] cubic axes, and is designated as $a^-a^-c^+$ in the space group *Pbnm* (#62; *cab* setting). For the compounds synthesized the mean ionic radius of the *A*-cations in eight-fold coordination ($^{viii}R_A$) decreases from 1.175 to 1.134 Å due to the lanthanide contraction, whereas the mean ionic radius of the *B*-site cations is constant at 0.623 Å. Thus, throughout the series the eight-fold coordination Goldschmidt tolerance factor (^{viii}t) decreases from 0.895 for the Pr-compound to 0.884 for the Tm-compound (Table 3).

Fig. 4 and Table 3 show that the unit cell volumes of the isostructural *Pbnm* $Na_{0.75}Ln_{0.25}Ti_{0.5}Nb_{0.5}$ compounds and unit cell parameters decrease throughout the series from Pr to Tm. In common with other $GdFeO_3$-type perovskites, these compounds have $a(\sim\sqrt{2}a_p)<b$ $(\sqrt{2}a_p)<c$ $(\sim 2a_p)$ and $a<c/\sqrt{2}<b$. However, Fig. 4 shows clearly that for the Pr and Nd compounds, $c/\sqrt{2}$ tends towards the value of the *b* cell dimension. This reflects the increasing $^{viii}R_A$ of the light lanthanide compounds, and suggests that a further increase in $^{viii}R_A$ will result in a composition driven phase transition. As $Na_{0.75}La_{0.25}Ti_{0.5}Nb_{0.5}$ has been shown to adopt space group *Cmcm*, we can predict that the transition from *Pbnm* to *Cmcm* structures must occur somewhere within the potential solid solution between the Pr, Ce and La compounds, and that the Ce compound ($^{xii}t = 0.968$) probably adopts the *Cmcm* structure.

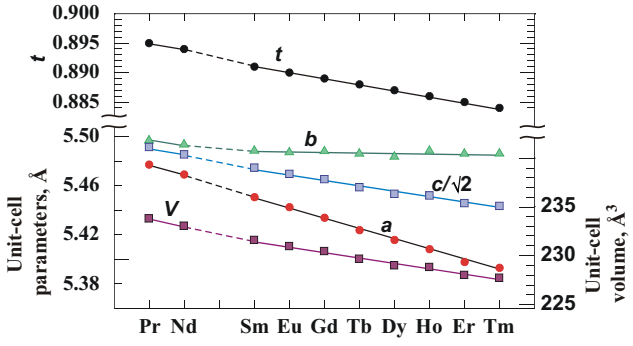

Fig. 4. Variation of Goldschmidt tolerance factor, unit-cell parameters and volumes for *Pbnm* $Na_{0.75}Ln_{0.25}Ti_{0.5}Nb_{0.5}O_3$ compounds. *Note*: where not seen, the error bars are less than the dot size employed for plotting (Table 3).

Typically, the coordination polyhedron of cations occupying the *A*-site of most ABO_3 orthoperovskites [1,10,11] is regarded as eight-fold (^{viii}A) rather than 12-fold (^{xii}A), i.e., a four-fold antiprism with eight short A–^{I}O(1,2) bonds in the first (I) coordination sphere of the *A*-cation. Four longer A–^{II}O(2) bonds give rise to the second (II) coordination sphere. The distortion of the AO_8 coordination polyhedron is also accompanied by displacement of the *A*-site cations from the center of the polyhedron (Table 3). Bond length analysis of the compounds synthesized shows that the *B*-site cation enters the second coordination sphere of the *A* cations

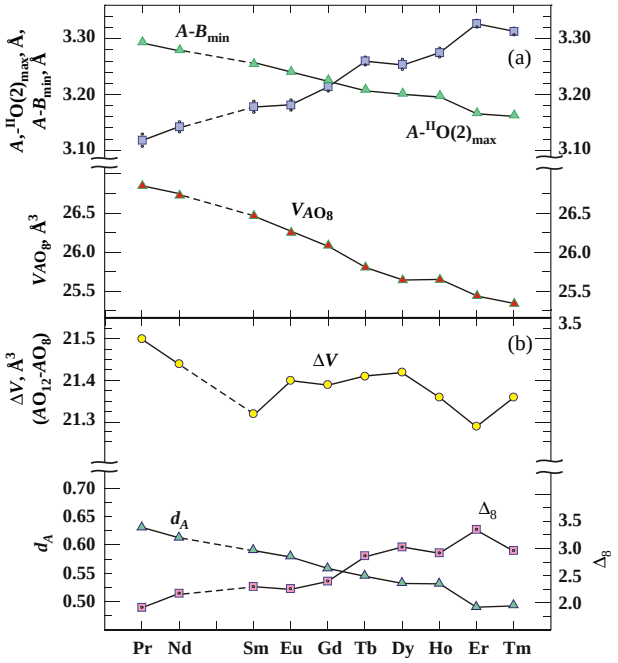

Fig. 5. Variation of bond lengths and polyhedral volumes for *Pbnm* $Na_{0.75}Ln_{0.25}Ti_{0.5}Nb_{0.5}O_3$ compounds. *Note*: where not seen, the error bars are less than the dot size employed for plotting (Tables 4 and 5).

for lanthanides heavier than Gd, as the maximum A–^{II}O(2) distances exceed the minimum A–B distances (Table 5, Fig. 5). This observation is robust as the estimated standard deviations of the bond lengths are far less than the difference between the longest A–^{II}O(2) bond and the minimum A–B distance.

The coordinations of compounds based on lanthanides lighter than Gd are not well-defined. Table 5 and Fig. 5 show that the B-cations lie outside of the second coordination sphere of the A-cations, as the A–B distances are greater than the maximum A–^{II}O(2) distances. The distance separating the first and second coordination spheres increases regularly from Gd to Pr (Table 5). This reflects the convergence of the $c/\sqrt{2}$ and b cell parameters and increase in average R_A leading ultimately to the formation of the 12-fold coordinated A-cations in the La compound. Bond valence analysis is not instructive with regard to the coordination problem as calculations for the Pr compound using IVTON and lanthanide bond valence parameters from [26] indicate significant underbonding for the both the A and B-site cations in twelve- and six-fold coordination, respectively. Inspection of the bond lengths (Table 5) suggests that the coordination of the Pr and Nd compounds is probably ten, whereas that of the Sm and Eu compounds remains at eight. Because of this uncertainty, note that for comparative purposes all crystallographic characteristics for the *Pbnm* compounds presented in Table 5 and Fig. 5 are based upon an assumed eight-fold coordination for the A-site cations.

Similar subtle changes in the coordination of A-site cations between the light and heavy lanthanide orthoferrites and orthoscandates have been documented by Marezio et al. [10] and Liferovich and Mitchell [11], and for the CaTiO–$NaTaO_3$ solid solution series [27].

As in other $GdFeO_3$-type perovskites, tilt angles increase as the size of the A-cation and the f-parameters decrease (Table 4). Because of the larger average A-site cationic radius of these compounds, tilt angles are less than those described for the corresponding ternary lanthanide orthoferrites and orthoscandates [10,11]. The mean bond $\langle B{-}O\rangle$ length and BO_6 volume change insignificantly throughout the series, and show an antipathetic correlation with the mean $\langle A{-}O\rangle$ and A-site volumes (Table 5).

The BO_6 bond length distortion indices (Δ_6) are higher than those of other lanthanide orthoperovskites [10]. These are unlikely to reflect the actual distortion of the BO_6 polyhedra because of the difficulties in locating precisely the positions of the atoms of oxygen by laboratory XRD methods. We consider that there is a systematic error in the determination of the O(1) and O(2) positions in these compounds leading to the anomalously low B–O(2) bond lengths given in Table 5. Regardless, we believe that the mean $\langle B{-}O\rangle$ bond lengths are realistic and that the A-site coordination analysis given above is valid.

6. Conclusions

The $Na_{0.75}La_{0.25}Ti_{0.5}Nb_{0.5}$ perovskite adopts space group *Cmcm*, whereas other ternary $Na_{0.75}Ln_{0.25}Ti_{0.5}Nb_{0.5}$ ($Ln = Pr$, Nd, Sm, Eu, Gd, Tb, Dy, Ho, Er, Tm) perovskites adopt the *Pbnm* $GdFeO_3$ structure, as consequence of the large ionic radius of La and high Goldschmidt tolerance factor ($^{xii}t = 0.97$) relative to that of other lanthanides (for Pr–Tm; $^{viii}t = 0.895$–0.884; $^{viii}t_o = 0.940$–0.902). The regular changes in cell dimensions and other crystallographic characteristics suggest that a continuous solid solution can exist between all of *Pbnm* structured perovskites synthesized, and that a compositionally-driven phase transition to a *Cmcm* structure will occur when lanthanides with an ionic radius less than that of Pr are replaced by significant amounts of La or Ce.

The $Na_{0.75}Ln_{0.25}Ti_{0.5}Nb_{0.5}$ compounds exhibit subtle changes in A-site cation coordination in response to the lanthanide contraction. Compounds based on Pr to Gd have B-site cations lying outside of the first and second coordination spheres of the A-site cations, whereas B-site cations in the Tb to Tm compounds enter the second coordination sphere of the A-site cations.

The $Na_{0.75}Ln_{0.25}Ti_{0.5}Nb_{0.5}$ compounds are stable phases at ambient conditions and might be considered as suitable for the sequestration of lanthanide fission

products such as ^{147}Pm, ^{151}Sm, ^{154}Eu, occurring in radioactive waste or Pu^{3+}, if $Na_{0.75}Pu_{0.25}Ti_{0.5}Nb_{0.5}$ is considered as a structural analog of $Na_{0.75}Gd_{0.25}Ti_{0.5}Nb_{0.5}$ ($^{viii}t = 0.889$). However, as the ^{viii}t factor for $Na_{0.75}Pu_{0.25}Ti_{0.5}Nb_{0.5}$ is 0.896, the Pr and Nd compounds, with ^{viii}t factors of 0.896 and 0.894, respectively, might be considered as the more appropriate analogs.

Our data also have a bearing on the crystal structures of naturally occurring members of the solid solution series $NaNbO_3$ (lueshite)–$NaLnTi_2O_6$ (loparite)–$SrTiO_3$ (tausonite) as these are known to be strongly dependent upon composition. For example, niobian calcian loparite is orthorhombic *Pbnm*, whereas strontian calcian loparite is tetragonal $I4/mcm$ [28], and lanthanian lueshite is cubic $Pm\bar{3}m$ [29]. The structures of the Ca- and Sr-poor lueshite-loparite series have not yet been determined. As the *A*-site in these minerals is dominated by Na, La and Ce, it is suggested that intermediate (50 mol%) members of the solid solution series $NaNbO_3$ (lueshite)–$NaLnTi_2O_6$ (loparite) should adopt the space group *Cmcm*. As loparite-rich compositions, and the compound $NaCeTi_2O_6$, are orthorhombic *Pbnm* [29,30], at least three compositionally-driven space group changes can be expected to occur within this series i.e., *Pbma* (#57) through *Cmcm* (#63) to *Pbnm* (#62). We are currently investigating the crystal structure of this solid solution series.

Acknowledgments

This work is supported by the Natural Sciences and Engineering Research Council of Canada and Lakehead University. Allan MacKenzie is acknowledged for assistance with the X-ray diffraction and microprobe work. Anne Hammond is thanked for sample preparation. The authors are grateful to three anonymous reviewers whose constructive criticism resulted in improvements to the initial version of the manuscript. The authors also would like to thank Dr. Matthew J. Rosseinsky for editorial care in handling this contribution.

References

[1] R.H. Mitchell, Perovskites: Modern and Ancient, Almaz Press, Thunder Bay, Ontario, Canada, 2002, 322pp. http://www.almazpress.com.
[2] P.H. Sun, T. Nakamura, Y.J. Shan, Y. Inaguma, M. Itoh, Ferroelectrics 200 (1997) 93.
[3] Y.J. Shan, T. Nakamura, Y. Inaguma, M. Itoh, Solid State Ionics 108 (1998) 123.
[4] A.E. Ringwood, S.E. Kesson, K.D. Reeve, D.M. Levins, E.J. Ramm, in: W. Lutze, R.C. Ewing (Eds.), Radioactive Waste Forms for the Future, North-Holland, Amsterdam, 1988.
[5] J.A. Purton, N.L. Allan, J. Mater. Chem. 12 (2002) 2923.
[6] C.N.W. Darlington, K.S. Knight, Acta Crystallogr. B 55 (1999) 24.
[7] A.C. Sakowski-Cowley, K. Lukaszewicz, H.D. Megaw, Acta Crystallogr. B 25 (1969) 851.
[8] R.H. Mitchell, A.R. Chakhmouradian, P.M. Woodward, Phys. Chem. Miner. 27 (2000) 583.
[9] A. Ahtee, M. Ahtee, A.M. Glazer, A.W. Hewat, Acta Crystallogr. B 26 (1976) 3243.
[10] M. Marezio, J.P. Remeika, P.D. Dernier, Acta Crystallogr. B 26 (1970) 2008.
[11] R.P. Liferovich, R.H. Mitchell, J. Solid State Chem. 177 (2004) 2188.
[12] A.A. Kern, A.A. Coelho, vol. 144, Allied Publishers Ltd., 1998, http://www.bruker-axs.com
[13] I.T. Balić-Žunić, I. Vicković, I. Appl. Crystallogr. 29 (1996) 305.
[14] R.D. Shannon, Acta Crystallogr. Sect. A 32 (1976) 751.
[15] K. Robinson, G.V. Gibbs, P.H. Ribbe, Science 172 (1971) 567–570.
[16] E. Dowty, Atoms 5.0, By Shape Software, Kingsport, TN 37663, USA, 1999.
[17] Y. Zhao, D.J. Weidner, J.B. Parise, D.E. Cox, Phys. Earth Planet. Interiors 76 (1993) 1.
[18] B.J. Kennedy, C.H. Howard, B.C. Chakoumakos, Phys. Rev. B 59 (1999) 4023.
[19] C.J. Howard, K.S. Knight, B.J. Kennedy, E.H. Kisi, J. Phys.: Condens. Matter 12 (2000) L677.
[20] B.J. Kennedy, K. Yamaura, E.J. Takayama-Muromachi, Phys. Chem. Solid 65 (2004) 1065.
[21] B.J. Kennedy, B.A. Hunter, J.R. Hester, Phys. Rev. B 65 (2002) 224103.
[22] L. Li, B.J. Kennedy, Y. Kubota, K. Kato, R.J. Garrett, Mater. Chem. 14 (2004) 263.
[23] B.J. Kennedy, A.K. Prodjosantoso, C.H. Howard, J. Phys.: Condens. Matter. 11 (1999) 1479.
[24] B.J. Kennedy, C.H. Howard, B.C. Chakoumakos, Phys. Rev. B 60 (1999) 2972.
[25] A.M. Glazer, Acta Crystallogr. Sect. B 28 (1972) 3384.
[26] A. Trzesowska, R. Kruszynski, T.J. Bartczak, Acta Crystallogr. B 60 (2004) 174.
[27] R.H. Mitchell, R.P. Liferovich, J. Solid State Chem. 177 (2004) 4420.
[28] R.H. Mitchell, P.C. Burns, A.R. Chakhmouradian, Canad. Mineral. 38 (2000) 145.
[29] S.V. Krivovichev, A.R. Chakhmouradian, R.H. Mitchell, R.H. Filatov, N.V. Chukanov, Eur. J. Mineral. 12 (2000) 597.
[30] A.R. Chakhmouradian, R.H. Mitchell, R.H. Pankov, N.V. Chukanov, Mineral. Mag. 63 (1999) 519.